Delineation of an oral cancer lesion with swept-source optical coherence tomography

Meng-Tsan Tsai
Hsiang-Chieh Lee
Chih-Wei Lu
Yih-Ming Wang
Cheng-Kuang Lee
C. C. Yang
National Taiwan University
Institute of Photonics and Optoelectronics
Department of Electrical Engineering
1 Roosevelt Road, Section 4
Taipei, Taiwan

Chun-Ping Chiang
National Taiwan University
Department of Dentistry
Taipei, Taiwan

Abstract. We demonstrate the *ex vivo* imaging of an oral cancerous sample with a swept-source optical coherence tomography (SS-OCT) system. With the axial resolution of 8 μm in free space and system sensitivity of 108 dB, we can well distinguish the normal and abnormal tissue portions in a sample. In particular, we analyze the lateral variation of A-scan profiles to show two parameters of SS-OCT signal for delineating an oral cancer lesion. One of the parameters is the decay constant in the exponential fitting of the SS-OCT signal intensity along depth. This decay constant decreases as the A-scan point moves laterally across the margin of a lesion. The other parameter is the standard deviation of the SS-OCT signal intensity fluctuation in an A-scan. This parameter increases significantly when the A-scan point is moved across the transition region between the normal and abnormal portions. Such parameters are useful for determining the margins of oral cancer.
[DOI: 10.1117/1.2960632]

Keywords: biomedical optics; coherent optical system; image analysis; imaging; scattering.

Paper 07397R received Sep. 24, 2007; revised manuscript received Jan. 8, 2008; accepted for publication Feb. 17, 2008; published online Aug. 8, 2008.

1 Introduction

The majority of oral cancers are found to develop from oral premalignant lesions such as leukoplakia, erythroplakia, erythroleukoplakia, dysplasia, and carcinoma *in situ*. The malignant transformation rates of oral premalignant lesions are reported to be 1% to 7% for homogenous, thick leukoplakia, 4% to 15% for granular or verruciform leukoplakia, 18% to 47% for erythroleukoplakia, 4% to 11% for moderate dysplasia, and 20% to 35% for severe dysplasia.[1] The high malignant transformation rates for oral premalignant lesions indicate the importance of early diagnosis and early treatment. For making a correct pathological diagnosis, a suspicious oral lesion may need multiple biopsies to avoid misdiagnosis of the most severe part of the lesion. To reduce the patient's pain and suffering from multiple biopsies, one of the best noninvasive ways to choose the most appropriate sites for biopsy is the use of optical coherence tomography (OCT)[2] for detecting oral precancers and cancers.[3] By using the interferometric cross-correlation technique to detect the coherent backscattered components of short-coherence-length light, OCT has become a powerful tool for the diagnoses of various diseases.[4,5] Pioneered by Puliafito et al.[6] to perform *in vivo* clinical imaging of the human eye, OCT has been an emerging bioimaging technology that promises to have broad and significant impact on clinical diagnostic imaging.

Although a variety of medical and biological applications have been developed based on the time-domain configuration of OCT, such a configuration has several restrictions, including the limited imaging speed.[7] Recently, OCT systems based on the Fourier-domain detection have been widely implemented. In such a system, either with the spectrometer configuration, which is normally called the spectral-domain OCT (SD-OCT),[8–11] or with a frequency-swept source, which is usually named the swept-source OCT (SS-OCT),[12–14] the OCT images are obtained through the measurement of the echo time delay of the backscattered light by spectrally resolving the interference signal. A Fourier-domain OCT system has the advantages of higher imaging sensitivity and higher imaging speed when compared with a time-domain system.[15–17] In the SD-OCT technique, normally a detector array, such as a charge-coupled device, is needed. The slow development of charge-coupled device has limited the application of the SD-OCT technique. On the other hand, the rapid development of a sweeping-frequency laser source has led to the spectral coverage of SS-OCT over the whole biological window, from 1300 nm (Ref. 13) through 1050 nm (Refs. 18–20) to 850 nm (Refs. 21 and 22). Nowadays, SS-OCT systems are widely used for various biomedical applications.

Optical coherence tomography has been widely used for studying oral cavity diseases.[23–31] It was used for imaging the oral carcinogenesis of a hamster cheek pouch model to discriminate the structural change in oral mucosa.[23,24,27] With the technique of optical Doppler tomography, the changes in axial blood flow velocity and the blood vessel size were also observed in an animal model.[25,29] Based on the development of a microelectromechanical system for fabricating a catheter, a three-dimensional-scan OCT system has been demonstrated

Address all correspondence to C. C. Yang, Institute of Photonics and Optoelectronics, Dept. of Electrical Engineering, National Taiwan University, 1 Roosevelt Rd., Section 4, Taipei, Taiwan, Republic of China. Tel: 886-2-23657624; Fax: 886-2-23652637; E-mail: ccy@cc.ee.ntu.edu.tw.

1083-3668/2008/13(4)/044012/6/$25.00 © 2008 SPIE

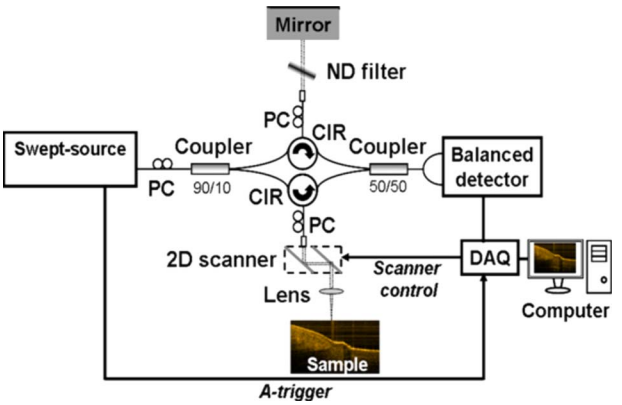

Fig. 1 Layout of the SS-OCT system. PC: polarization controller, CIR: circulator.

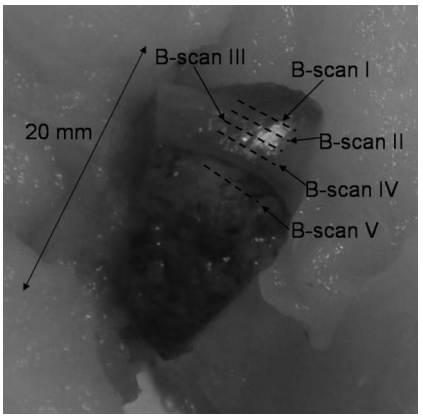

Fig. 2 Picture of the oral cancer sample used for study. The portion at the upper-left corner consists of normal tissue. The positions of the five SS-OCT B-scans are indicated.

for early detection and diagnosis of oral premalignancy and malignancy.[26,28] Meanwhile, by using the Muller matrix analysis, the difference of optical features between noncancerous and precancerous tissues could be observed.[30] Due to the high-resolution, high-sensitivity, and high-speed scanning features, it has been widely demonstrated that OCT is suitable for clinical oral cavity scanning.[3,31]

In both the diagnosis and therapy of oral cancer, it is important to know the margin of an oral cancer lesion. A misjudgment of the margin will lead to the misinterpretation of cancer condition or incomplete therapy. In this paper, we first demonstrate the *ex vivo* imaging capability of an oral cancerous sample with an SS-OCT system. We then analyze the lateral variation of an A-scan profile to show two parameters of OCT signal for determining the margin of abnormal tissue. One of the parameters is the decay constant in the exponential fitting of the OCT signal intensity along the depth. The other parameter is the standard deviation of the OCT signal intensity fluctuation in an A-scan. Such parameters are believed to be useful for delineating an oral cancer lesion. In Sec. 2, we describe the structure and parameters of the SS-OCT system used. The general OCT scanning results are presented in Sec. 3. Then, we discuss the analyses of the lateral variation of the A-scan profile across the transition region from the normal to abnormal tissue portions in Sec. 4. Finally, conclusions are drawn in Sec. 5.

2 SS-OCT System

Figure 1 shows the layout of the SS-OCT system, which is in a standard fiber-based SS-OCT configuration. A sweeping-frequency laser source (HSL-2000, Santec Corp., Hackensack, New jersey) of 1310 nm in central wavelength, 100 nm in spectral full width at half maximum, and a scanning rate of 20 kHz, which leads to a 20 frames/s imaging rate, is used. The maximum output power is 6 mW. The theoretical axial resolution of the SS-OCT system is 7 μm in free space. However, because of the residual dispersion effect of the system, the implemented axial resolution is 8 μm in free space. The output of the light source is connected to a Mach-Zehnder interferometer consisting of two couplers and two circulators. To optimize the system sensitivity, a 10/90 coupler is used to reduce the power loss in the reference arm and increase the incident power onto the sample. In addition, a continuously tunable neutral density filter is introduced into the reference arm to maximize the sensitivity. A system sensitivity of 108 dB is achieved. In the sample arm, a two-axis galvanometer (Cambridge Technology, Lexington, Massachusetts) is used to provide two- or three-dimensional scanning. The interfered signal is detected by a balanced photodetector configuration and sampled by a high-speed digitizer (PXI-5122, National Instruments, Austin, Texas). Before being Fourier-transformed into the spatial domain, the interfered signal spectrum is rescaled to have an evenly spaced frequency interval by using the phase-oriented fringe analysis technique.[32] With this software technique, no additional equipment is required. The dispersion is compensated by a software compensation scheme.[10] The rescaled spectral signal is then passed through a digital Hamming window to shape the spectrum and pad zero to 2048 points. After the inverse Fourier transform, an A-scan profile of 1024 pixels can be acquired.

3 *Ex vivo* Scanning Results

In the *ex vivo* study, we chose a piece of cancerous buccal mucosa for SS-OCT scanning. Figure 2 shows the picture of the sample, which has a dimension of roughly 20×13 mm. A small portion at the upper-left corner, which is thinner than the rest of the sample, consists of normal tissue. Cancerous tissues can be clearly seen in the two-thirds portion of the lower-right corner. Therefore, an OCT B-scan along the direction from upper left to lower right may cover a transition range from the normal to abnormal portions. The positions of the five SS-OCT B-scans (B-scans I to V) are indicated in Fig. 2. B-scan V covers completely cancerous tissue. Figure 3 shows three histology images of the sample close to the locations of B-scans I (a), IV (b), and V (c). The normal, abnormal, and cancerous portions are roughly circled and indicated. In this figure, we use the term of "cancerous" to differentiate from the evolving abnormal tissue. The increasing thickness of the epithelium (EP) layer and the diminishing boundary between the EP and lamina propria (LP) layers represent the first indicator of tissue abnormality that may eventually evolve into cancerous tissue. In Figure 3(a), one can see that the thickness of the EP layer increases from the left to the

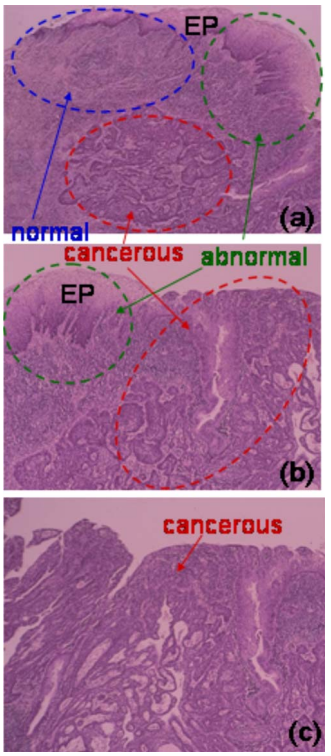

Fig. 3 Histology images of the same oral cancer sample. The structures of parts (a) to (c) were obtained from the locations close to B-scans I, IV, and V, respectively. The normal, abnormal, and cancerous portions are roughly circled and indicated. The whole area of part (c) covers cancerous tissue.

right portion of the image. Also, the boundary between the EP and LP layers becomes unclear at the very right end. Abnormal tissues exist in the two-thirds area of the lower-right corner. In Fig. 3(b), cancerous tissues cover the whole image except a small area in the upper-left corner. In this area, the EP layer is quite thick and the boundary is unclear, indicating that the tissue is evolving into the cancerous condition. In part (c), it is quite clear that the whole image covers cancerous tissues.

Figure 4 shows four SS-OCT scan images of the sample corresponding to B-scans I to IV. The four images were taken about 1 mm apart as shown in Fig. 2. At the left ends of B-scans I to IV, no tissue image was acquired because of the large curvature of sample surface there. In B-scan I, when the tissue image appears, first the boundary between the EP and LP layers can be clearly identified. However, the boundary diminishes as we scan the sample toward the right end. This trend is also quite clear in B-scans II to IV. One can see that the transition from the normal portion at the upper-left corner to the abnormal portion at the lower-right corner of the sample does not have a clear boundary. In this situation, it is difficult for a physician to delineate the lesion and perform precise incision or excision. Therefore, understanding the lateral variations of OCT signal features across the margin of a lesion is important for oral cancer diagnosis and therapy.

4 Image Analysis Results and Discussions

Figures 5(a) and 5(b) show the OCT images of B-scans I and V, respectively. Four vertical lines, labeled with 1 through 4,

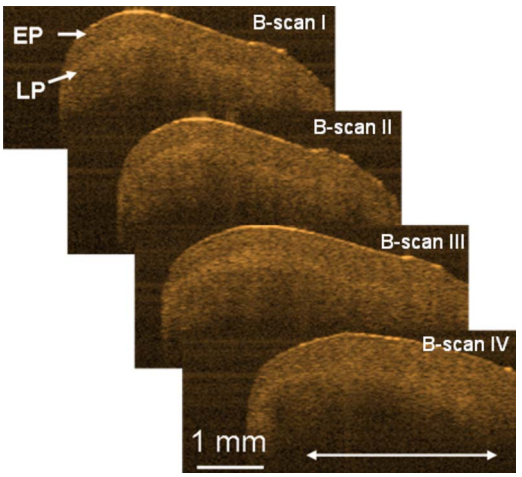

Fig. 4 The SS-OCT scanning images of the oral cancer sample at the locations of B-scans I to IV.

indicate the A-scan results to be analyzed. The OCT signals of those A-scans are shown in Fig. 6 in a range from the sample surface down to 2100 μm in depth. In the A-scan 1, at which the tissue is supposed to be normal, beside the peak at the air/tissue interface, there is a peak around 400 μm in depth corresponding to the boundary between the EP and LP layers. This peak and the relatively weaker signal intensity fluctuations in the EP and LP layers represent the features of healthy oral mucosa. In A-scan 2, the signal peak around 330 μm in depth becomes relatively less prominent and the signal intensity fluctuation becomes stronger. These variation trends become clearer in A-scans 3 and 4, in which the boundaries between the EP and LP layers disappear and the OCT signal intensity fluctuations are quite strong. These trends indicate that from A-scans 1 through 4, the scan point moves across the margin of the lesion. The exponential fitting curves of the OCT signal intensity in the whole depth range for the four A-scan profiles of Fig. 6 are plotted for calibrating the intensity decay constants. The calibrated exponential decay

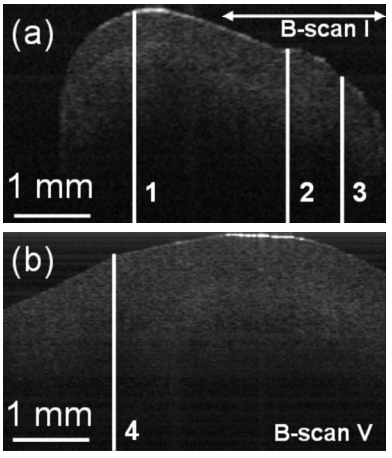

Fig. 5 The SS-OCT images of B-scans I (a) and V (b) for detailed analysis. The four A-scans, denoted by the four vertical lines (labeled 1 through 4) are to be analyzed. The horizontal two-way arrow shows the lateral range of the data in Fig. 7.

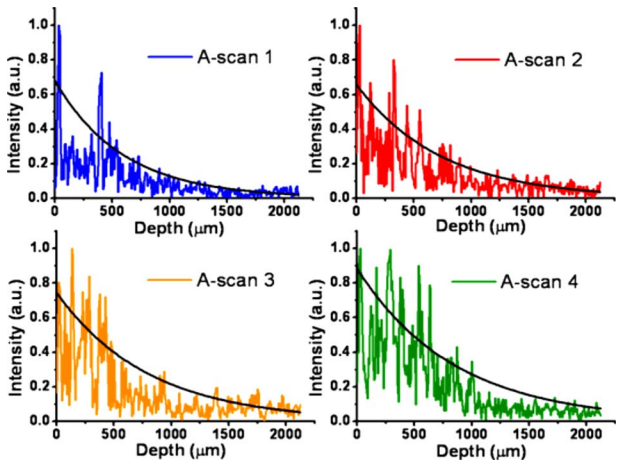

Fig. 6 The SS-OCT signal intensity profiles of A-scans 1 through 4. The curves across the intensity fluctuations show the exponential fitting.

constants are 0.0119, 0.0096, 0.0088, and 0.0084 μm^{-1} for A-scans 1 through 4, respectively. The fittings show the decreasing trend of the depth decay constant as the scan point moves across the margin into the abnormal portion. This trend is further manifested in Fig. 7, in which the exponential decay constant of OCT signal intensity is plotted as a function of lateral scan distance in a range of B-scan I, as indicated by the horizontal two-way arrow at the upper-right corner of Fig. 5(a). In Fig. 7, one can see that in spite of the fluctuation and the two sharp peaks around 1300 and 1800 μm in lateral scan distance, the calibrated decay constant shows a decreasing trend and can become negative. A negative decay constant means a generally increasing trend of OCT signal intensity along depth in the concerned depth range. The two peaks correspond to the lateral positions where strongly scattered spots can be identified on the sample surface, as can be clearly seen in Fig. 5(a). In Fig. 7, a third-order polynomial fitting curve is plotted to show the decreasing trend of decay constant. The lateral variation of decay constant as shown in Fig. 7 can be used as an indicator for determining the margin of abnormal tissue. Figure 8 shows similar curves to those in Fig. 7 for a range of B-scan IV, as indicated by the horizontal

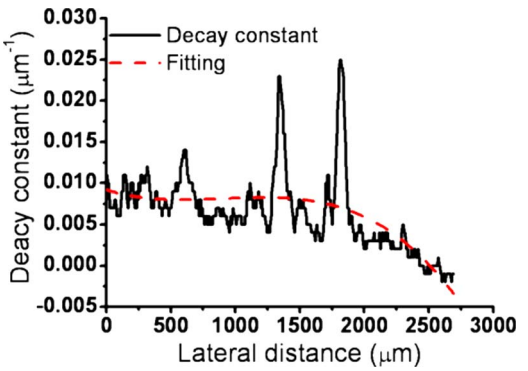

Fig. 7 The SS-OCT signal intensity decay constant as a function of lateral distance obtained from the exponential fitting, which is demonstrated in Fig. 6, in the range indicated by the horizontal two-way arrow in Fig. 5(a) of B-scan I.

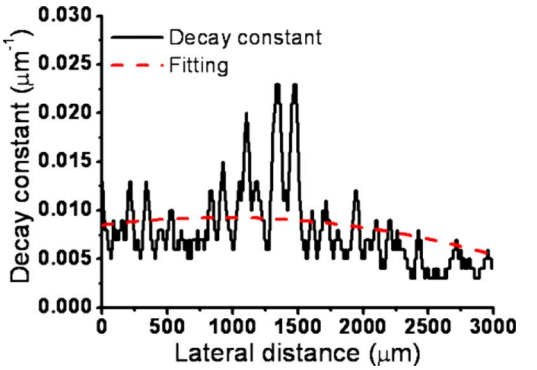

Fig. 8 The SS-OCT signal intensity decay constant as a function of lateral distance in the range indicated by the horizontal two-way arrow in Fig. 4 of B-scan IV.

two-way arrow in Fig. 4. In this figure, several spikes, particularly those between 800 and 1500 μm, disturb the variation trend of decay constant such that the margin of the abnormality based on this trend is shifted toward the left. Hence, the decay constant trend may become inaccurate for determining the margin of a lesion when strong backscattering spots exist on sample surface. Nevertheless, this trend can still provide us an approximate margin of a lesion.

The other useful indicator for determining the margin of abnormal tissue is the fluctuation extent of OCT signal intensity in an A-scan. Figure 9 shows the signal intensity fluctuations in the presumable range of the EP layer (300-μm depth from the surface in this calibration) of the four A-scans shown in Figs. 5(a) and 5(b). Each curve in Fig. 9 was obtained by removing the data point on the sample surface and shifting the average level to 0 in each A-scan. Here, one can see that among the four curves, A-scan 1 has the smallest fluctuation with the standard deviation of 0.079. As the scan point moves toward the cancerous portion, the fluctuation becomes stronger and stronger. The standard deviations of A-scans 2 through 4 become 0.1588, 0.2298, and 0.2277, respectively. The level of standard deviation can also be used for determining the margin of abnormal tissue. Figure 10 shows the variation of standard deviation as a function of lateral distance along B-scan IV in the same range as that of Fig. 8. From the data and the fitting curve, one can clearly see the increasing

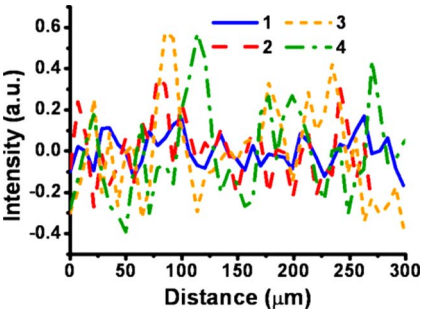

Fig. 9 The SS-OCT signal intensity fluctuations of the four A-scans, 1 through 4, in the range of 300 μm from the sample surface after the peaks at the sample surface are removed and the average levels are shifted to 0.

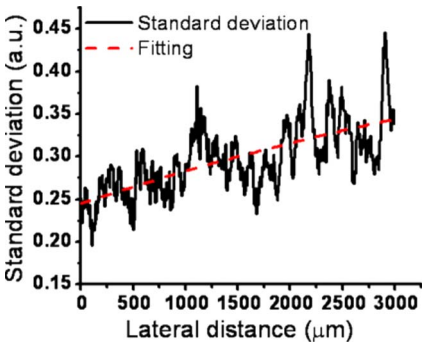

Fig. 10 Variation of the standard deviation of the SS-OCT signal intensity fluctuation in an A-scan, as a function of lateral distance along B-scan IV.

trend when the scan point moves toward the cancerous portion. This result indicates that the whole scan range of Figs. 8 and 10 actually covers abnormal tissue.

Normally, an oral precancerous lesion has an inhomogeneous distribution, That is, part of the lesion may show only benign hyperkeratosis and acanthosis, but the other part may include dysplasia, carcinoma *in situ*, or an early invasive carcinoma. In making a diagnosis of an oral precancerous lesion, we usually select the most severe part of the lesion for incisional biopsy. Also, in a surgical excision, we need to determine the safety margin of an oral cancer to prevent the local recurrence of the oral cancer. The previously described image process, based on the demonstrated analyses of the SS-OCT scanning results, can help us in the selection of the most severe part of a lesion and the determination of the safety margin for surgical excision. Such analyses for finding the margins are useful for the diagnosis and therapy of oral cancer.

5 Conclusions

In summary, we have demonstrated the *ex vivo* imaging of an oral cancerous sample with an SS-OCT system. With the axial resolution of 8 μm in free space and system sensitivity of 108 dB, we could distinguish normal and abnormal tissues. Based on the SS-OCT data, we analyzed the lateral variation of A-scan profiles to show two parameters for determining the margin of an oral cancer lesion. The first parameter was the decay constant in the exponential fitting of the OCT signal intensity along depth. This decay constant decreased as the A-scan point moved laterally across the margin of a lesion. The second parameter was the standard deviation of the OCT signal intensity fluctuation in an A-scan. This parameter increased significantly when an A-scan was performed in the abnormal portion of a sample.

Acknowledgment

This research was supported by National Health Research Institute, the Republic of China, under Grant No. NHRI-EX96-9616EI. Dr. Kwang-Yu Hu of the Far Eastern Memorial Hospital, Taipei, Taiwan, is appreciated for providing us with cancerous oral mucosa specimens.

References

1. B. W. Neville, D. D. Damm, C. M. Allen, and J. E. Bouquot, "Epithelial Pathology," in *Oral Maxillofacial Pathology*, pp. 259–321, W. B. Sauders, Philadelphia (1995).
2. D. Huang, E. A. Swanson, C. P. Lin, J. S. Schuman, W. G. Stinson, W. Chang, M. R. Hee, T. Flotte, K. Gregory, C. A. Puliafito, and J. G. Fujimoto, "Optical coherence tomography," *Science* **254**, 1178–1181 (1991).
3. J. M. Ridgway, W. B. Armstrong, S. Guo, U. Mahmood, J. Su, R. P. Jackson, T. Shibuya, R. L. Crumley, M. Gu, Zhongping Chen, and B. J.-F. Wang, "*In vivo* optical coherence tomography of the human oral cavity and oropharynx," *Arch. Otolaryngol. Head Neck Surg.* **132**, 1074–1081 (2006).
4. M. R. Lee, J. A. Izatt, E. A. Swanson, D. Huang, J. S. Schumun, C. P. Lin, C. A. Puliafito, and J. G. Fujimoto, "Optical coherence tomography for ophthalmic imaging: new technique delivers micron-scale resolution,"*IEEE Eng. Med. Biol. Mag.* **14**, 67–76 (1995).
5. J. G. Fujimoto, M. E. Brezinski, G. T. Tearney, S. A. Boppart, B. E. Bouma, M. R. Hee, J. F. Southern, and E. A. Swanson, "Biomedical imaging and optical biopsy using optical coherence tomography," *Nat. Med. (N.Y.)* **1**, 970–972 (1995).
6. C. A. Puliafito, M. R. Hee, J. S. Schuman, and J. G. Fujimoto, *Optical Coherence Tomography of Ocular Diseases*, SLACK, Thorofare, N.J. (1996).
7. G. J. Tearney, B. E. Bouma, and G. J. Fujimoto, "High-speed phase- and group-delay scanning with a grating-based phase control delay line," *Opt. Lett.* **22**, 1811–1813 (1997).
8. A. F. Fercher, C. K. Hitzenberger, G. Kamp, and S. Y. Elzaiat, "Measurement of intraocular distances by backscattering spectral interferometry," *Opt. Commun.* **117**, 43–48 (1995).
9. S. Yun, G. Tearney, B. Bouma, B. Park, and J. de Boer, "High-speed spectral-domain optical coherence tomography at 1.3 μm wavelength," *Opt. Express* **11**, 3598–3604 (2003).
10. M. Wojtkowski, V. Srinivasan, T. Ko, J. Fujimoto, A. Kowalczyk, and J. Duker, "Ultrahigh-resolution, high-speed, Fourier domain optical coherence tomography and methods for dispersion compensation," *Opt. Express* **12**, 2404–2422 (2004).
11. B. Cense, N. Nassif, T. Chen, M. Pierce, S.-H. Yun, B. Park, B. Bouma, G. Tearney, and J. de Boer, "Ultrahigh-resolution high-speed retinal imaging using spectral-domain optical coherence tomography," *Opt. Express* **12**, 2435–2447 (2004).
12. B. Golubovic, B. E. Bouma, G. J. Tearney, and J. G. Fujimoto, "Optical frequency-domain reflectometry using rapid wavelength tuning of a Cr4+:forsterite laser," *Opt. Lett.* **22**, 1704–1706 (1997).
13. S. H. Yun, G. J. Tearney, J. F. de Boer, N. Iftimia, and B. E. Bouma, "High-speed optical frequency-domain imaging," *Opt. Express* **11**, 2953–2963 (2003).
14. R. Huber, D. C. Adler, and J. G. Fujimoto, "Buffered Fourier domain mode locking: unidirectional swept laser sources for optical coherence tomography imaging at 370,000 lines/s," *Opt. Lett.* **31**, 2975–2977 (2006).
15. J. F. de Boer, B. Cense, B. H. Park, M. C. Pierce, G. J. Tearney, and B. E. Bouma, "Improved signal-to-noise ratio in spectral-domain compared with time-domain optical coherence tomography," *Opt. Lett.* **28**, 2067–2069 (2003).
16. R. Leitgeb, C. K. Hitzenberger, and A. F. Fercher, "Performance of Fourier domain vs. time domain optical coherence tomography," *Opt. Express* **11**, 889–894 (2003).
17. M. A. Choma, M. V. Sarunic, C. H. Yang, and J. A. Izatt, "Sensitivity advantage of swept source and Fourier domain optical coherence tomography," *Opt. Express* **11**, 2183–2189 (2003).
18. E. C. Lee, J. F. de Boer, M. Mujat, H. Lim, and S. H. Yun, "*In vivo* optical frequency domain imaging of human retina and choroid," *Opt. Express* **14**, 4403–4411 (2006).
19. Y. Yasuno, Y. Hong, S. Makita, M. Yamanari, M. Akiba, M. Miura, and T. Yatagai, "*In vivo* high-contrast imaging of deep posterior eye by 1-μm swept source optical coherence tomography and scattering optical coherence angiography," *Opt. Express* **15**, 6121–6139 (2007).
20. J. Zhang, Q. Wang, B. Rao, Z. Chen, and K. Hsu, "Swept laser source at 1 μm for Fourier domain optical coherence tomography," *Appl. Phys. Lett.* **89**, 073901 (2006).
21. V. J. Srinivasan, R. Huber, I. Gorczynska, J. G. Fujimoto, J. Y. Jiang, P. Reisen, and A. E. Cable, "High-speed, high-resolution optical coherence tomography retinal imaging with a frequency-swept laser at 850 nm," *Opt. Lett.* **32**, 361–363 (2007).

22. H. Lim, J. F. de Boer, B. H. Park, E. C. Lee, R. Yelin, and S. H. Yun, "Optical frequency domain imaging with a rapidly swept laser in the 815–870 nm range," *Opt. Express* **14**, 5937–5944 (2006).
23. P. Wilder-Smith, W. Jung, M. Brenner, K. Osann, H. Beydoun, D. Messadi, and Z. Chen, "*In vivo* optical coherence tomography for the diagnosis of oral malignancy," *Lasers Surg. Med.* **35**, 269–275 (2004).
24. E. Matheny, N. Hanna, W. Jung, Z. Chen, and P. Wilder-Smith, "Optical coherence tomography of malignancy in hamster cheek punches," *J. Biomed. Opt.* **9**, 978–981 (2004).
25. P. Wilder-Smith, T. Krasieva, W. Jung, J. Zhang, Z. Chen, K. Osann and B. Tromberg, "Noninvasive imaging of oral premalignancy and malignancy," *J. Biomed. Opt.* **10**, 051601 (2005).
26. W. Jung, J. Zhang, J. Chung, P. Wilder-Smith, M. Brenner, J. S. Nelson, and Z. Chen, "Advances in oral cancer detection using optical coherence tomography," *IEEE J. Sel. Top. Quantum Electron.* **11**, 811–817 (2005).
27. T. M. Muanza, A. P. Cotrim, M. McAuliffe, A. L. Sowers, B. J. Baum, J. A. Cook, F. Feldchtein, P. Amazeen, C. N. Coleman, and J. B. Mitchell, "Evaluation of radiation-induced oral mucositis by optical coherence tomography," *Clin. Cancer Res.* **11**, 5121–5127 (2005).
28. N. Hanna, W. Waite, K. Taylor, W. G. Jung, D. Mukai, E. Matheny, K. Kreuter, P. Wilder-Smith, M. Brenner, and Z. Chen, "Feasibility of three-dimensional optical coherence tomography and optical Doppler tomography of malignancy in hamster cheek pouches," *Photomed. Laser Surge.* **24**, 402–409 (2006).
29. P. Wilder-Smith, M. J. Hammer-Wilson, J. Zhang, Q. Wang, K. Osann, Z. Chen, H. Wigdor, J. Schwartz, and J. Epstein, "*In vivo* imaging of oral mucositis in an animal model using optical coherence tomography and optical Doppler tomography," *Clin. Cancer Res.* **13**, 2449–2454 (2007).
30. J. Chung, W. Jung, M. J. Hammer-Wilson, P. Wilder-Smith, and Z. Chen, "Use of polar decomposition for the diagnosis of oral precancer," *Appl. Opt.* **46**, 3038–3045 (2007).
31. H. Kawakami-Wong, S. Gu, M. J. Hammer-Wilson, J. B. Epstein, Z. Chen, and P. Wilder-Smith, "*In vivo* optical coherence tomography-based scoring of oral mucositis in human subjects: a pilot study," *J. Biomed. Opt.* **12**, 051702 (2007).
32. Y. Yasuno, V. D. Madjarova, S. Makita, M. Akiba, A. Morosawa, C. Chong, T. Sakai, K. P. Chan, M. Itoh, and T. Yatagai, "Three-dimension and high-speed swept-source optical coherence tomography for *in vivo* investigation of human anterior eye segments," *Opt. Express* **13**, 10652–10664 (2005).